

Directed Self-Assembly of Block Copolymers on Two-Dimensional Chemical Patterns Fabricated by Electro-Oxidation Nanolithography

By Ji Xu, Soojin Park, Shiliu Wang, Thomas P. Russell,* Benjamin M. Ocko,* and Antonio Checco*

In the bulk, block copolymers (BCPs) self assemble into ordered morphologies, having spherical, cylindrical, lamellar, or bicontinuous gyroid microdomains, where the molecular weight of the BCP dictates the sizes of the microdomains formed. In thin films, controlling the orientation and lateral ordering of the microdomains has enabled the use of these morphologies as templates and scaffolds for the fabrication of nanostructured materials. Thin films of BCPs have been used as templates to fabricate quantum dots,^[1] nanowires,^[2–4] magnetic storage media,^[5] nanopores,^[6,7] and silicon capacitors.^[8] For applications where addressability is desired it is mandatory to control both the orientation and lateral ordering of the microdomains. Numerous methods have been developed to control the orientation and lateral ordering, including the use of electric,^[9] shear,^[10] thermal,^[11] and solvent fields,^[12–14] as well as, zone casting,^[15] controlled interfacial interactions,^[16] surface topography,^[17–19] and chemical patterning.^[20–23] Both linear^[16] and complex 2D topographical features have been used to orient the BCP domains. Chemical patterning is particularly appealing, since it can provide a contrast in the interfacial interactions without topographic features. Initial studies of templated BCP films using chemical patterns have used linear features. Rockford et al.^[20] used Au stripes on faceted silicon surfaces whereas Kim et al.^[22] used chemical stripes patterned using extreme UV lithography and soft X-ray oxidation of a phenyl-terminated self-assembled monolayer (SAM). These studies have shown that the linear patterns can be used to provide detailed control of the commensuration and

orientation of the lamellar BCP phase. Subsequently, Kim et al.^[22] have shown that similar patterns can also be used to create 1D arrays of BCP cylinders. In this work, both blocks of the BCP interact non-favorably with the hydrophobic substrate that produces an orientation of the BCP microdomains normal to the surface. More recently, density multiplication using chemical patterns has been successfully used to develop long-range order in BCP films.^[19,24,25] This method selectively pins single BCP domains rather than using patterns of parallel lines to create linear arrays of BCP domains. To date, chemical patterns have not been used to pin the BCP domains within complex 2D geometries.

In this work, we demonstrate an approach to direct the self-assembly of BCPs within complex 2D geometries by using chemical patterns. The boundaries of the patterns are used to pin and template the order of the BCP domains, whereas the pattern geometry is chosen to improve the spatial uniformity of the domains. The chemical patterns are fabricated using oxidative nanolithography, where the metal-coated tip of an atomic force microscopy (AFM) instrument is used to oxidize the terminal methyl groups of a SAM into carboxylic acid groups. The chemical contrast between the patterned (polar) and unpatterned (nonpolar) regions can be used to control the BCP interfacial interactions, which dictates the orientation of the microdomains. A particularly attractive feature of this process is that there is no topography on the surface and only the different chemical functionalities of the surface guide the BCP ordering. In the present case, the polymer film would dewet the ultralow-energy methyl-terminated regions, however the presence of the surrounding carboxylic acid-terminated regions stabilize the film from dewetting. Compared to the phenyl-terminated SAM used by Kim et al.,^[26] the methyl-terminated SAM used here has a much lower surface energy. As such, the polymer films more strongly dewet the unpatterned methyl regions than the unpatterned phenyl regions used by Kim et al.^[26]

Polished silicon (100) wafers (*p* doped, resistivity below 100 Ωcm) with their native oxide layer were coated with a SAM of octadecyltrichlorosilane (OTS) by immersion in a 5 mM solution of OTS in toluene.^[27] This monolayer is composed of well-packed, fully extended, methyl-terminated hydrocarbon chains, 2.5 nm thick, as determined by X-ray reflectivity. The 113° and 103° contact angle of water, for the respective advancing and receding directions provides additional support for well-packed layer.^[27] In addition, AFM images show that the surface of the monolayer is defect-free with negligible roughness.

[*] Dr. A. Checco, Dr. B. M. Ocko
Condensed Matter Physics and Materials Science Department
Brookhaven National Laboratory
Upton, NY 11973 (USA)
E-mail: checco@bnl.gov; ocko@bnl.gov
Prof. T. P. Russell, J. Xu
Department of Polymer Science and Engineering
University of Massachusetts Amherst
120 Governors Drive, Amherst MA 01003 (USA)
E-mail: russell@mail.pse.umass.edu
Prof. S. Park
School of Energy Engineering
Ulsan National Institute of Science and Technology
100 Banyeon-ri, Eonyang-eup, Ulju-gun, Ulsan (Korea)
S. Wang
Deerfield Academy
Deerfield, MA 01342 (USA)

DOI: 10.1002/adma.200903640

To carry out the electro-oxidation nanolithography we used an Agilent 5500 AFM that is contained in a humidity controlled chamber. A metallic, biased contact-mode AFM tip (MicroMasch, CSC17) was used to electrochemically oxidize the terminal methyl groups of the monolayer to carboxylic acid groups under high-humidity conditions.^[28] The resulting chemical patterns exhibit a very weak height contrast (~ 0.3 nm) and are more clearly imaged by using friction force mode, as shown in Figure 1. The boundary between patterned and unpatterned regions is not perfectly sharp. Rather it has a finite width as a result of the diffusive motion of the oxidizing species produced in proximity of the tip apex. The full-width-half-maximum equivalent width, as measured by AFM in friction mode, is about 10 nm, which is comparable to the lateral roughness of the center of the boundary (measured over a length of about one micrometer).

The polymer thin film was prepared using polystyrene-*block*-poly(ethylene oxide) (PS-*b*-PEO)); (Polymer Source) with an average molecular weight of 26.5 kg mol^{-1} , where the polystyrene (PS) weight fraction is ~ 0.76 and the polydispersity is about 1.06. The polymer film with a 25–30 nm thickness, measured by ellipsometry, was spin-cast onto the patterned substrate from a 10 mg mL^{-1} dimethyl formamide solution. The sample was then annealed for around 18 h at 150°C under high vacuum. To improve the phase contrast in tapping-mode AFM the sample was soaked in ethanol for 5 min and then purged with dry nitrogen. This “reconstruction process” selectively dissolves the poly(ethylene oxide) (PEO) block which exposes more PEO to the top surface.^[29,30]

Representative AFM images of the surface reconstructed sample are shown in Figure 2 for a polymer film on an OTS surface patterned with equally spaced, ~ 200 -nm-wide, carboxylic lines in both height (a) and phase-contrast modes (b). The topography image clearly shows that the polymer film covers both the patterned and unpatterned regions. The corresponding cross-sectional profile in (c) shows that the film thickness is not uniform. On the methyl-terminated regions the film thickness is

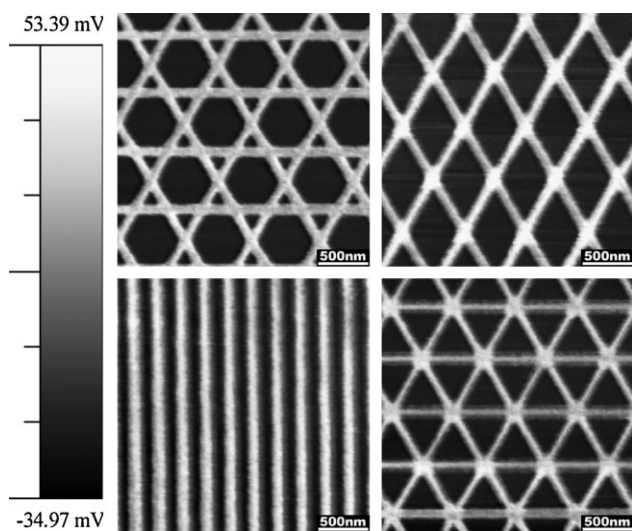


Figure 1. AFM friction-mode images of chemical patterns of various geometries: hexagons (top-left), diamonds (top-right), triangles (bottom-right), and stripes (bottom-left).

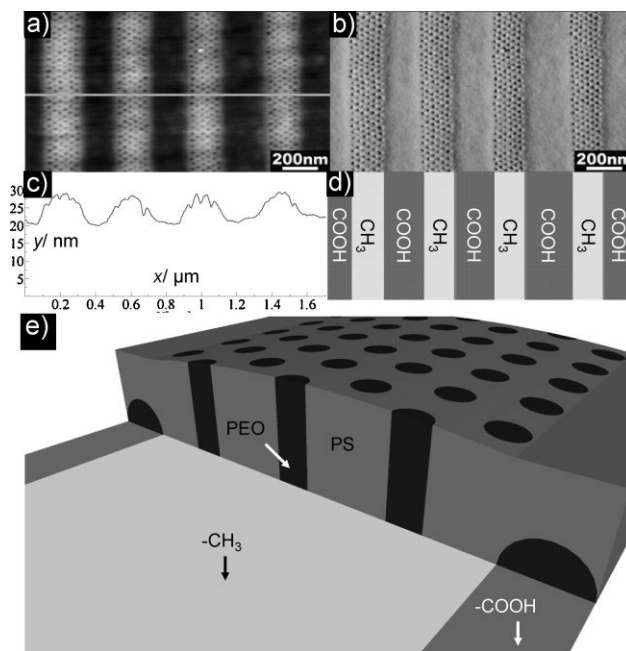


Figure 2. a) Height and b) phase images in tapping-mode AFM of annealed and surface-reconstructed PS-*b*-PEO on stripe patterns. In the phase image the bright and dark regions correspond to the PS layer and PEO microdomains, respectively. c) Height profile of the film measured along the solid line shown in (a). d) Representation of the alternating methyl- and carboxylic acid-terminated stripes underlying the film shown in (a,b). e) Schematic images of the internal structure of the annealed film covering the chemical patterns.

about 28 nm, which is thicker than the 20 nm thickness measured on the carboxylic regions. A hexagonal pattern with a lattice constant of ~ 29 nm is observed in both topography and phase pictures over the methyl-terminated regions. In contrast, the carboxylic acid-terminated regions appear featureless. Together these results suggest that the PEO cylinders stand normal to the surface on the unpatterned regions, whereas on the patterned regions the PEO block is pinned to the substrate leaving the PS block at the free surface with a “brush-like” structure. The latter results from the attractive interaction between the PEO and carboxylic acid-terminated regions. The different copolymer morphologies on the patterned and unpatterned regions are schematically shown in Figure 2e.

The orientation of the PEO block on the methyl-terminated surface depends on interfacial interactions and on how the film thickness differs from its bulk equilibrium period $L_0 \approx 30 \mu\text{m}$ (discussed below). To quantify the first factor we have measured the contact angle of micrometer-sized annealed PS and PEO droplets on an OTS surface by AFM, obtaining $62 \pm 1^\circ$ and $60 \pm 3^\circ$, respectively (see the Supporting Information Fig. S1). This result suggests that the interfacial energies of the two blocks in contact with the OTS surface are very similar and therefore the methyl-terminated monolayer acts as a neutral surface for the two polymer components. Meanwhile, the two blocks share a very similar value of surface tension, 31.3 and 34.7 mN m^{-1} for PS and PEO, respectively, at elevated temperature (150°C) utilized for annealing, and this interface is also nearly neutral. This neutral

wetting condition for the two polymer components promotes a perpendicular orientation of BCP microdomains.^[31] In addition to the neutral wetting condition, the film thickness may also help promote a perpendicular orientation. This is because a non-integer number of parallel oriented PEO cylinders is energetically unfavorable. In the present case the film thickness is slightly less than the L_0 . Our results show that chemical patterning alone, even in the absence of topography, is effective in controlling the orientation and the spatial ordering of BCP domains on surfaces that the BCP would otherwise dewet. Consequently, the orientation of the microdomains normal to the film surface, in our experiments, results from a situation where interfacial interactions of the two blocks are equally non-favorable. The considerations above provide support for the structural model described in Figure 2e, which is also consistent with simulations by Kim et al.^[26] Direct experimental evidence for the 3D structure of the films on the methyl-terminated patterns could be obtained, for example, by imaging cross-sections of the films with scanning electron microscopy (SEM). Unfortunately, in our case it is quite difficult to produce cross-sections of the sample because the patterns cover a very limited portion of the substrate and, hence, it is difficult to crack the sample exactly in the middle of the patterns. To overcome these limitations, we have prepared substrates patterned with a very large number of micrometer-sized, circular OTS regions following a procedure detailed in the Experimental section and schematized in Figure S3 of the Supporting Information. In this case, cross-sections of annealed polymer films covering the circular OTS regions can be easily obtained by cracking the sample. Images of the sample cross-sections by SEM reveal that the cylindrical microdomains on the OTS-coated regions extend vertically throughout the film (see Fig. S4 of the Supporting Information).

An important finding from this study is that the sharp boundary between the patterned and nonpatterned regions very effectively templates the order of the cylindrical microdomains. This is demonstrated by Figure 2a and 2b which show that the PEO microdomains are aligned along the outline of the stripe pattern. Therefore, the templating action of the pattern boundary can be used as a “corral” to confine the BCP microdomains within well-defined patterned regions.

The corral concept is illustrated by Figure 3a where the methyl-terminated hexagonal patterned regions have been used to laterally confine the cylindrical microdomains thus forming defect-free crystals (see Fig. 3b). All geometries with hexagonal symmetry (hexagons, triangles, diamonds, and stripes) were effective to control the orientation of the microdomain lattice (Fig. 3b–e). To better visualize the point defects, we applied a Voronoi diagram, which is constructed by

drawing the bonds connecting a microdomain with all its neighbors.^[32] The perpendicular bisectors of these bonds intersect to form polygons. A polygon has a number of sides equal to the number of nearest neighbors of the microdomain in the center. While six-fold-coordinated sites are denoted as white hexagons whereas the five, seven, and eight-fold-coordinated sites are denoted as dark gray pentagons, black heptagons and gray octagons, respectively. The Voronoi diagrams in Figure 3b'–e' indicate that an almost defect-free array lattice exists in each of those geometries. The geometries shown in Figure 3 have dimensions of around $10L_0$ and similar results were observed in smaller geometries. To study the extent to which the pattern size can be increased without introducing a significant number of defects we made hexagonal patterns with various sizes (the longest diagonal in a hexagon) ranging from ~ 500 to ~ 1500 nm. When the diameter is smaller than $1 \mu\text{m}$, the pattern is either defect-free (Fig. 4a and 4a') or contains only a small number of defects (Fig. 4b, 4b', 4c, and 4c'). As the diameter increases, the number of point defect increases, thereby destroying the long-range order of the nano-arrays (Fig. 4d, 4d', 4e, and 4e'). In comparison, a PS-*b*-PEO thin film deposited on a silicon wafer and annealed for a similar period of time

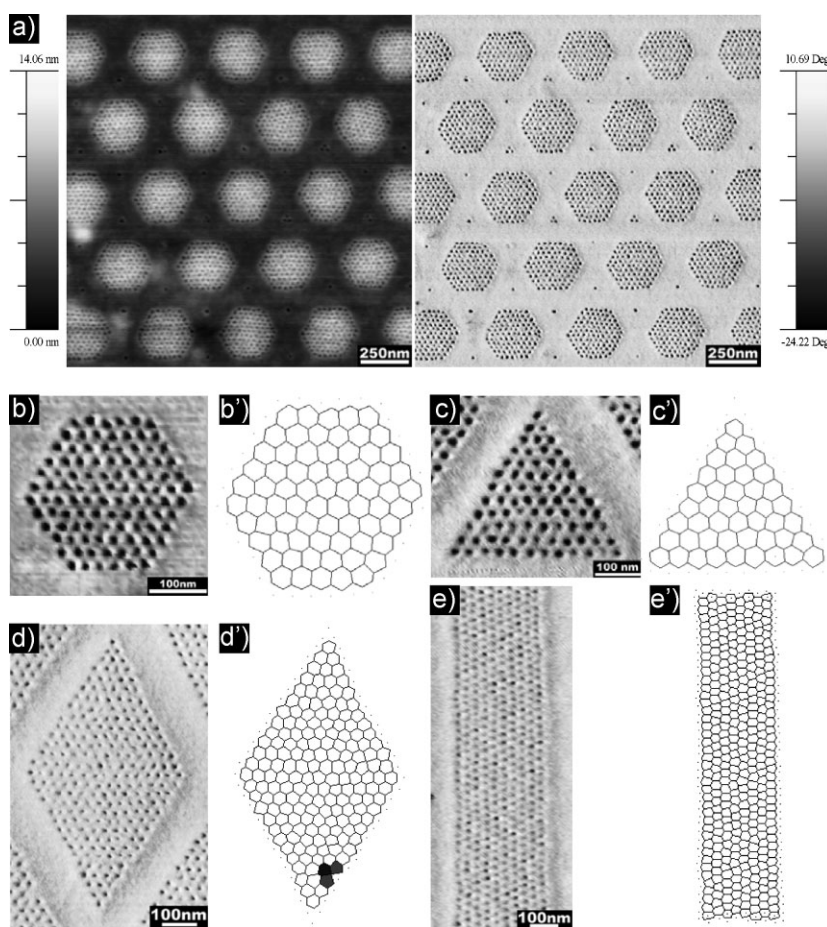


Figure 3. a) Height (left) and phase (right) tapping-mode AFM images of annealed PS-*b*-PEO films on hexagonally shaped, web-like patterns. Phase images of films covering hexagonal (b), triangular (c), diamond-like (d), and striped (e) methyl-terminated patterns and corresponding Voronoi diagrams b'–e').

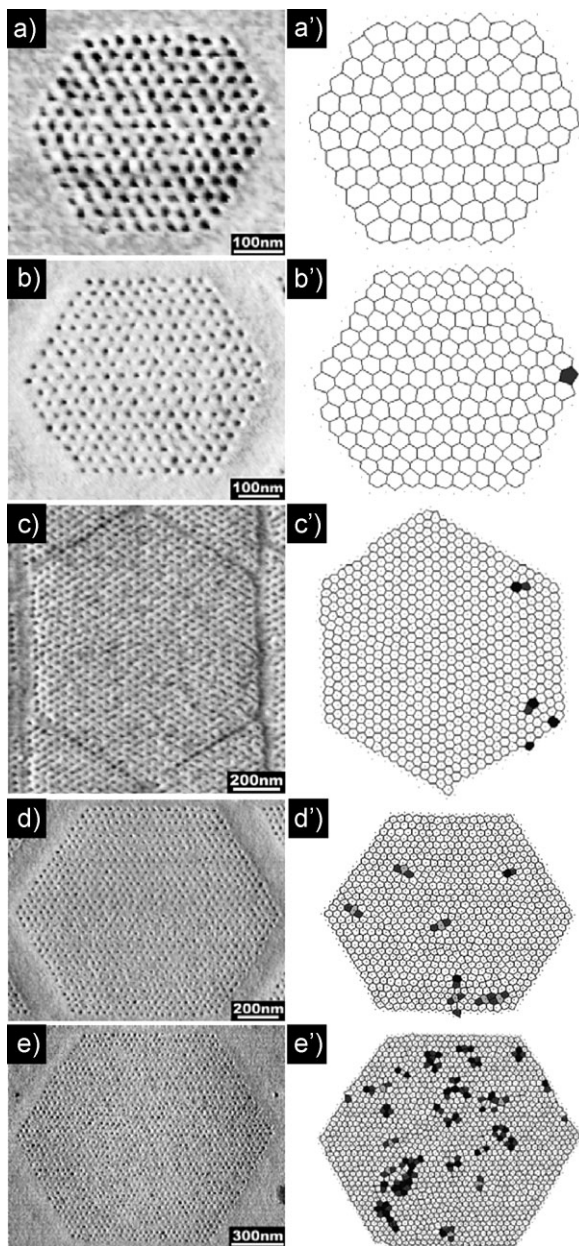


Figure 4. Tapping-mode AFM phase images of annealed PS-*b*-PEO films on hexagonal, methyl-terminated patterns of diameter equal to: a) 500 nm, b) 600 nm, c) 1175 nm, d) 1300 nm, and e) 1500 nm and corresponding Voronoi diagrams (a'–e', respectively).

exhibits “polycrystalline” microdomains consisting of randomly oriented ordered grains of sizes ranging from ~ 500 nm to about $1 \mu\text{m}$. Thus, besides controlling the orientation of the BCP microdomain lattice, the hexagonal-shaped chemical patterns are also effective in suppressing the formation of grain boundaries and increasing the grain size.

Our method provides a versatile approach to build hierarchical structures on chemical patterns for different BCP systems. Considering that the surface tension of poly(methylmethacrylate) (PMMA) (31.2 mN m^{-1}) is very close to that of PS at 150°C , we

conjectured that similar confinement effects might occur with PS-*b*-PMMA instead of PS-*b*-PEO. To test this possibility we performed similar experiments using a cylinder-forming PS-*b*-PMMA ($M_n = 60 \text{ k}$, $\omega_{\text{PS}} = 0.74$, $\text{PDI} = 1.06$) anionically synthesized in our laboratory. Under the same film preparation and annealing conditions, except that a benzene/hexane (50:50 v/v) solution instead of dimethylformamide solution was applied during spin-coating, we have obtained hierarchical structures very similar to PS-*b*-PEO (see the Supporting Information, Fig. S2). Imaging of the sample cross-section by SEM reveals that the PMMA cylindrical microdomains on the OTS-coated regions extend vertically throughout the film (see Fig. S4 of the Supporting Information).

In conclusion, we have shown that chemical patterns are as effective as topographical patterns for templating the BCP microdomains in thin films, resulting in well-packed microdomain arrays with long-range order. These patterns exhibit two surface chemistries, which promote different orientations of the BCP microdomains, while the sharp boundaries of the pattern template the order of the microdomains. The combined sectoring and self-assembly provides a unique route toward the hierarchical assembly of BCP films with long-range order. By using parallel patterning with arrays of AFM cantilevers^[33] or stamping with large-scale conductive stamps,^[34] this approach could be exploited for the fabrication of patterned media for high-density magnetic storage or microelectronic applications.^[8]

Experimental

Surface Modification of Silicon Substrates: In a nitrogen-purged glove box, polished silicon (100) wafers (*p* doped, resistivity below $100 \Omega\text{cm}$) with their native oxide layer were immersed in a solution of OTS in toluene (5 mmol L^{-1}) for 24 h. Afterwards, wafers were sonicated in toluene for 5 min, rinsed multiple times with chloroform and cleaned with a jet of supercritical carbon dioxide (snow jet). X-ray reflectivity, grazing incidence X-ray scattering, FTIR, and contact-angle measurements have been used to insure that the OTS layers are of the highest quality.

Electro-oxidation Nanolithography: An Agilent 5500 AFM that is contained in a humidity controlled chamber was used to carry out the electro-oxidation nanolithography. A metallic, biased contact-mode AFM tip (MicroMasch, CSC17) was used to electrochemically oxidize the terminal methyl groups of the monolayer on the substrate to carboxylic acid groups under high-humidity conditions [28]. Contact-Mode AFM was performed immediately after each patterning process to image the patterns and confirm pattern quality.

Material, Thin Film Preparation, Thickness Measurement, and Thermal Annealing: PS-*b*-PEO ($M_n = 26.5 \text{ kg mol}^{-1}$, $\omega_{\text{PS}} = 0.76$, $\text{PDI} = 1.06$) was purchased from Polymer Source Inc. and used as received. PS-*b*-PMMA ($M_n = 60 \text{ kg mol}^{-1}$, $\omega_{\text{PS}} = 0.74$, $\text{PDI} = 1.06$) was synthesized in lab via anionic polymerization. Thin films were spin-cast onto the patterned substrates from a PS-*b*-PEO solution in dimethylformamide and a PS-*b*-PMMA solution in benzene/hexanes (1:1 v/v), respectively. A film thickness in the range 25–30 nm, as measured by ellipsometry (Rudolf Research), was obtained by carefully selecting the solution concentration and the spinning rate. Subsequently, samples were annealed at 150°C under high vacuum for 18 h and then quenched to room temperature.

AFM Imaging of Polymer Films: Tapping-mode AFM was performed on annealed polymer samples with a Veeco Dimension 3100 Scanning Probe Microscope.

Contact-Angle Measurements: PS ($M_n = 21 \text{ kg mol}^{-1}$, $\text{PDI} = 1.04$) and PEO ($M_n = 6 \text{ kg mol}^{-1}$, $\text{PDI} = 1.05$) were purchased from Polymer Source and used as received. Thin films (from 40 to 80 nm thick) of PS and PEO

were prepared by spin-coating onto OTS-modified silicon substrates and subsequently thermally annealing at 150 °C for 12 h in high vacuum. The annealed PS and PEO films are unstable and rupture into an array of micrometer-sized droplets, which exhibit a spherical cap shape as imaged by tapping-mode AFM. The contact angle (θ) of the droplet was estimated according to the relationship $\theta = 2\arctan(H/R)$ where H and R are height and radius of the droplet, respectively. The reported contact-angle values represent an average over at least 10 measurements on different droplets.

Preparation of Samples for Cross-Sectional SEM Imaging: A large number of circular OTS domains (sized between 0.5 and 2 μm) embedded in a hydrophilic substrate were prepared as described schematically in Fig. S3 of the Supporting Information. A 10 mg mL⁻¹ PS (3 k) solution in a solvent mixture of benzene/hexanes (50:50 v/v) was spin-cast at 3000 rpm onto an OTS-coated substrate. The film was then annealed at 150 °C under vacuum until it dewetted the OTS surface, breaking up into numerous circular PS droplets. The substrate was then exposed to oxygen plasma for 3 min to degrade the OTS film that was not protected by the PS drops, which rendered it hydrophilic. Subsequently, the substrate was rinsed in THF to remove the PS drops, dried, and cleaned using snow-jet. A \sim 30-nm-thick PS-*b*-PMMA (60 k) thin film was then spin-coated on the patterned substrate and annealed under vacuum for 20 h. The annealed film was irradiated with UV light (5.7 mW cm⁻²) under vacuum for 40 min to degrade the PMMA cylinders and simultaneously crosslink the PS chains. The film was then developed in acetic acid, which removes the PMMA cylinders leaving a porous PS template. The sample was cracked and subsequently coated with a \sim 3-nm-thick platinum layer by using a Gatan High-Resolution Ion Beam Coater (Model 681) at a sample tilt angle of 45° relative to source. The cross-section of the sample was imaged using a JEOL JSM-7001F scanning electron microscope and a representative image is shown in Figure S4 of the Supporting Information.

Acknowledgements

The authors are grateful to Qijun Xiao for help with SEM measurements. The work at the University of Massachusetts is supported by the MRSEC (Materials Research Science and Engineering Center) (J.X.), the Department of Energy Basic Energy Science (T.P.R.), FENA (Center on Functional Engineered Nano Architectonics) (S.P.), and the WCU program. Work at Brookhaven National Laboratory is supported by the U.S. Department of Energy, Division of Materials Science, under contract no. DE-AC02-98CH10886. Supporting Information is available online from Wiley InterScience or from the authors.

Received: October 23, 2009

Revised: December 1, 2009

Published online: April 6, 2010

- [1] M. Park, C. Harrison, P. M. Chaikin, R. A. Register, D. H. Adamson, *Science* **1997**, 276, 1401.
- [2] T. Thurn-Albrecht, J. Schotter, C. A. Kastle, N. Emley, T. Shibauchi, L. Krusin-Elbaum, K. Guarini, C. T. Black, M. T. Tuominen, T. P. Russell, *Science* **2000**, 290, 2126.
- [3] H. C. Kim, X. Q. Jia, C. M. Stafford, D. H. Kim, T. J. McCarthy, M. Tuominen, C. J. Hawker, T. P. Russell, *Adv. Mater.* **2001**, 13, 795.
- [4] W. A. Lopes, H. M. Jaeger, *Nature* **2001**, 414, 735.
- [5] J. Y. Cheng, C. A. Ross, V. Z. H. Chan, E. L. Thomas, R. G. H. Lammertink, G. J. Vancso, *Adv. Mater.* **2001**, 13, 1174.
- [6] V. Z. H. Chan, J. Hoffman, V. Y. Lee, H. Iatrou, A. Avgeropoulos, N. Hadjichristidis, R. D. Miller, E. L. Thomas, *Science* **1999**, 286, 1716.
- [7] M. J. Fasolka, A. M. Mayes, *Annu. Rev. Mater. Res.* **2001**, 31, 323.
- [8] C. T. Black, K. W. Guarini, K. R. Milkove, S. M. Baker, T. P. Russell, M. T. Tuominen, *Appl. Phys. Lett.* **2001**, 79, 409.
- [9] T. Thurn-Albrecht, J. DeRouchey, T. P. Russell, H. M. Jaeger, *Macromolecules* **2000**, 33, 3250.
- [10] D. E. Angelescu, J. H. Waller, D. H. Adamson, P. Deshpande, S. Y. Chou, R. A. Register, P. M. Chaikin, *Adv. Mater.* **2004**, 16, 1736.
- [11] J. Bodycomb, Y. Funaki, K. Kimishima, T. Hashimoto, *Macromolecules* **1999**, 32, 2075.
- [12] M. Kimura, M. J. Misner, T. Xu, S. H. Kim, T. P. Russell, *Langmuir* **2003**, 19, 9910.
- [13] S. Ludwigs, A. Boker, A. Voronov, N. Rehse, R. Magerle, G. Krausch, *Nat. Mater.* **2003**, 2, 744.
- [14] S. H. Kim, M. J. Misner, T. Xu, M. Kimura, T. P. Russell, *Adv. Mater.* **2004**, 16, 226.
- [15] C. B. Tang, A. Tracz, M. Kruk, R. Zhang, D. M. Smilgies, K. Matyjaszewski, T. Kowalewski, *J. Am. Chem. Soc.* **2005**, 127, 6918.
- [16] P. Mansky, Y. Liu, E. Huang, T. P. Russell, C. Hawker, *Science* **1997**, 275, 1458.
- [17] R. A. Segalman, H. Yokoyama, E. J. Kramer, *Adv. Mater.* **2001**, 13, 1152.
- [18] J. Y. Cheng, C. A. Ross, E. L. Thomas, H. I. Smith, G. J. Vancso, *Appl. Phys. Lett.* **2002**, 81, 3657.
- [19] I. Bitá, J. K. W. Yang, Y. S. Jung, C. A. Ross, E. L. Thomas, K. K. Berggren, *Science* **2008**, 321, 939.
- [20] L. Rockford, Y. Liu, P. Mansky, T. P. Russell, M. Yoon, S. G. J. Mochrie, *Phys. Rev. Lett.* **1999**, 82, 2602.
- [21] X. M. Yang, R. D. Peters, P. F. Nealey, H. H. Solak, F. Cerrina, *Macromolecules* **2000**, 33, 9575.
- [22] S. O. Kim, H. H. Solak, M. P. Stoykovich, N. J. Ferrier, J. J. de Pablo, P. F. Nealey, *Nature* **2003**, 424, 411.
- [23] L. Rockford, S. G. J. Mochrie, T. P. Russell, *Macromolecules* **2001**, 34, 1487.
- [24] R. Ruiz, H. M. Kang, F. A. Detcheverry, E. Dobisz, D. S. Kercher, T. R. Albrecht, J. J. de Pablo, P. F. Nealey, *Science* **2008**, 321, 936.
- [25] K. C. Daoulas, M. Muller, M. P. Stoykovich, H. Kang, J. J. de Pablo, P. F. Nealey, *Langmuir* **2008**, 24, 1284.
- [26] S. O. Kim, B. H. Kim, D. Meng, D. O. Shin, C. M. Koo, H. H. Solak, Q. Wang, *Adv. Mater.* **2007**, 19, 3271.
- [27] R. Maoz, S. R. Cohen, J. Sagiv, *Adv. Mater.* **1999**, 11, 55.
- [28] A. Checco, Y. G. Cai, O. Gang, B. M. Ocko, *Ultramicroscopy* **2006**, 106, 703.
- [29] T. Xu, J. Stevens, J. A. Villa, J. T. Goldbach, K. W. Guarini, C. T. Black, C. J. Hawker, T. P. Russell, *Adv. Funct. Mater.* **2003**, 13, 698.
- [30] S. Park, J. Y. Wang, B. Kim, J. Xu, T. P. Russell, *ACS Nano* **2008**, 2, 766.
- [31] Y. L. P. Mansky, E. Huang, T. P. Russell, C. Hawker, *Science* **1997**, 275, 1458.
- [32] R. A. Segalman, A. Hexemer, R. C. Hayward, E. J. Kramer, *Macromolecules* **2003**, 36, 3272.
- [33] C. Liu, *Mater. Today* **2008**, 11, 22.
- [34] S. Hoepfner, R. Maoz, J. Sagiv, *Nano Lett.* **2003**, 3, 761.